Spatial coherence of prepulse-induced neonlike x-ray lasers

Peixiang Lu,[1,*] Ernst Fill,[1] Yuelin Li,[1,†] Joachim Maruhn,[2] and Georg Pretzler[1]
[1]*Max-Planck-Institut für Quantenoptik, D-85740 Garching, Germany*
[2]*Institut für Theoretische Physik, Universität Frankfurt, D-60054 Frankfurt, Germany*
(Received 26 January 1998)

We report a series of Young's double-slit experiments to measure the transverse spatial coherence of prepulse-induced low-Z neonlike x-ray lasers for two prepulse levels. The experiments were performed using the Asterix IV iodine laser with a prepulse 5 ns before the main pulse. The main pulse energy was 400 J, with a pulse duration of 450 ps. Two slit separations of 80 and 110 μm were used to measure coherence in the vertical direction. We also present data for the horizontal transverse coherence, obtained with only a single-slit separation of 110 μm. The equivalent incoherent source sizes of the x-ray lasers along the vertical direction, as derived by the Van Cittert-Zernike theorem, were found to be 100–120 μm for the 1.5% prepulse, and 110–170 μm for the 15% prepulse level, respectively. Compared to the near-field patterns, the equivalent source sizes obtained with the lower prepulse level (1.5%) are found to be significantly smaller, indicative of an enhancement of the spatial coherence by the gain medium. The observation of a higher degree of coherence for the 1.5% prepulse is corroborated by simulations using a two-dimensional hydrocode and a ray-tracing postprocessor. [S1050-2947(98)00207-8]

PACS number(s): 42.55.Vc, 42.60.By, 32.30.Rj, 52.50.Jm

I. INTRODUCTION

Since the first demonstration of a collisionally pumped neonlike soft-x-ray laser in selenium [1,2], great progress has been achieved in extending the range of neonlike lasers and in characterizing their properties [3,4]. Recently, the application of a prepulse [5,6] has made it possible to generate strong emission on the $J=0-1$ lasing line in low- to moderate-Z elements ranging from Si ($Z=14$) to Se ($Z=34$) [7–10]. Using this technique, saturated $J=0-1$ neonlike Zn and Ge lasers at 21.2 and 19.6 nm have been demonstrated [11,12].

One of the most important parameters of soft-x-ray lasers is their spatial coherence, a knowledge of which is decisive for applications such as interferometry and holography [3,13–15]. Spatial coherence properties of x-ray lasers have been measured for materials including Zn [16], Ge [17,18], and Se [19,20]. Increasing coherence with increasing gain length has been demonstrated for a neonlike Ar laser pumped by a capillary discharge [21]. In these measurements, incoherent slit arrays [19,20], double slits [18], wires [17], and knife edges [16,21] were used as the diffracting elements. Similar techniques have been applied to measure the spatial coherence of extreme ultraviolet (XUV) lasers [22], a laser-plasma x-ray source [23], and of high-order harmonics generated in a gas [24] and on a solid surface [25].

In this paper, we report on comparative measurements of the transverse spatial coherence of prepulse-induced neonlike $J=0-1$ lasers in Ti, Cr, Fe, and Zn for the two different prepulse-to-main-pulse ratios of 1.5% and 15%. We also present data for several lasing lines of Ge for a 15% prepulse, which can be compared to recently published results [18].

We use the method of Young's double-slit interferometry to measure the spatial coherence. The interference patterns are compared to the ones of an incoherently radiating circular disk. Measured near-field patterns of our lasers are shown and related to the equivalent incoherent emitters. Simulations for the two prepulse levels are carried out using a two-dimensional (2D) hydrodynamic code coupled to a ray tracing code. It is found that most of the experimentally observed features are reproduced by the simulations. Deviations from experimental findings are attributed to simplified assumptions in the numerical model. The main observation, viz. a higher degree of coherence of the lower prepulse level, is corroborated by the theory.

II. EXPERIMENTAL SETUP

The experiments were carried out at the Asterix IV iodine laser facility [26]. This laser, with a beam diameter of 30 cm, was focused by a cylindrical lens array [27] to generate a 150-μm-wide and 3-cm-long line focus, yielding a 20-TW/cm^2 irradiance on the target surface with a 400-J 450-ps pulse. To produce a well-defined prepulse, part of the beam was deflected to propagate along a shorter distance in front of the final steering mirror. The delay between the main pulse and the prepulse was set to 5 ns. The energy ratio of the prepulse to the main pulse was 1.5% or 15%, which could be selected by inserting or removing a 10% neutral density filter into the beam path between the two mirrors generating the prepulse. All targets used in the experiments were planar 2.5-cm long slabs.

The criteria for using a Young's-type interference experiment for coherence measurements were formulated by

*Present address: NTT Basic Research Laboratories, Kanagawa, 243-0198 Japan.
†Present address: Lawrence Livermore National Laboratory, Livermore, CA 94550.

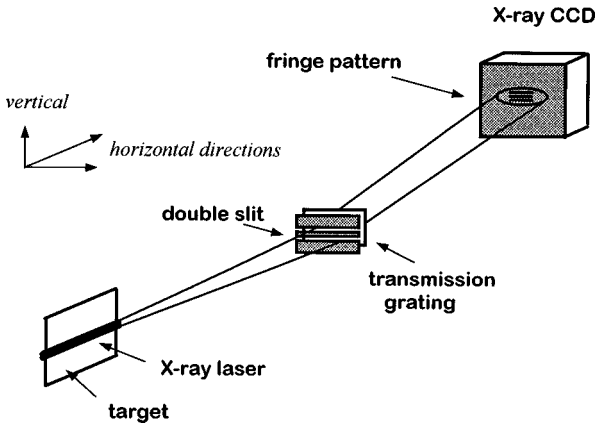

FIG. 1. Oblique drawing of the diagnostic setup to measure the vertical transverse spatial coherence of soft-x-ray lasers. The x-ray laser beam is horizontally emitted and is spectrally dispersed in the vertical direction by a 1000 l/mm transmission grating. A horizontally oriented slit pair is overlaid on the grating. The fringe pattern is recorded in first order by an x-ray CCD. The distances from the target to the double slit and from the double slit to the CCD are 65 and 75 cm, respectively. To measure the horizontal spatial coherence, the unit grating and double slit pair are rotated by 90°, and the x-ray CCD is moved into the first order again.

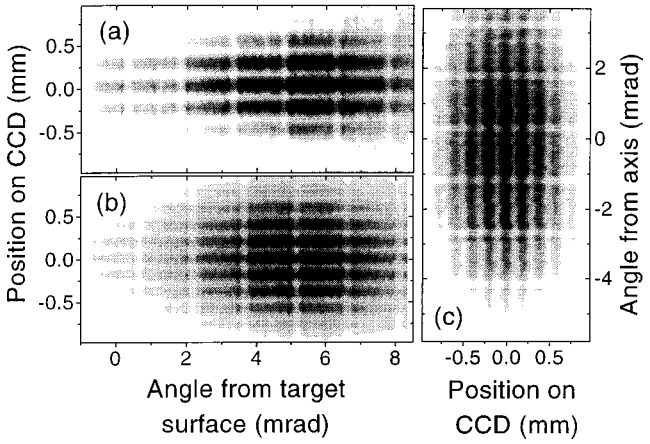

FIG. 2. Angularly resolved interference fringe image of the neonlike $J=0-1$ Fe x-ray laser at 25.5 nm. (a) Horizontal orientation of the grating bars and double-slit pair; 80-μm slit separation. (b) Horizontal orientation of the grating bars and double-slit pair; 110-μm slit separation. (c) Vertical orientation of the grating bars and double slit pair; 110-μm slit separation. The structure appearing in a direction perpendicular to the interference fringes is due to supporting bars of the transmission grating.

Nugent and Trebes [28]. We used a pair of 20-μm-wide slits,[1] placed 65 cm away from the target (see Fig. 1). Two different slit pairs with distances of 80 and 110 μm between the slits were employed. In order to separate the x-ray laser emission from the plasma background radiation, the axial plasma emission was spectrally dispersed by means of a transmission grating (1000 lines/mm), with the grating bars oriented parallel to the double slits. Fringe patterns at the peak of the angularly resolved emission of the x-ray lasers are recorded by an x-ray charge-coupled-device (CCD) camera 75 cm away from the double-slit pair.

The main part of the data was taken with the slits oriented horizontally, thus measuring the coherence in the vertical direction (i.e., parallel to the target surface). A less complete set of data with vertically oriented slits, with only one slit separation (110 μm), will also be presented.

III. EXPERIMENTAL RESULTS

As an example for the raw data obtained, the CCD readout for the case of Fe x-ray lasers with a 1.5% prepulse is shown in Fig. 2. The figure represents data taken with the 80- and 110-μm pairs in the horizontal direction, and with the 110-μm slit pair in the vertical direction. It illustrates the high visibility of the fringes for this laser, and the slight variation of the visibility along the angularly resolved direction. The substructure perpendicular to the interference pattern [i.e., the vertical structure in Figs. 2(a) and 2(b) and the horizontal structure in Fig. 2(c)] results from supporting bars of the transmission grating. Figure 3 shows the CCD readout obtained for Ti and Cr with a 15% prepulse. One sees that the fringe visibility is high at the peak of the emission, but deteriorates as one goes away from that direction. Again the vertical structure in this pattern is due to supporting bars of the transmission grating.

Spectra for Ti, Cr, Fe, and Zn at the peak of the angularly resolved emission are shown in Figs. 4(a) and 4(b). The figure compares 1.5% and 15% prepulses for the 80- and 110-μm horizontally oriented slit pairs. The corresponding patterns with 110-μm slit separation with vertical slits are shown in Fig. 5.

We further show interference patterns for Ge in the horizontal and vertical direction, for a single slit separation of 110 μm and a prepulse level of 15% (Fig. 6). The figure displays vertical and horizontal interference patterns for the $J=0-1$ line at 19.6 nm, the two $J=2-1$ lines at 23.2 and 23.6 nm, and for another $J=2-1$ line at 28.6 nm. The 23.2-

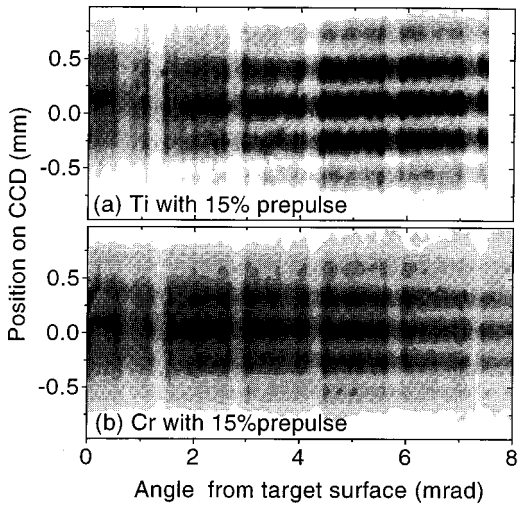

FIG. 3. Angularly resolved interference fringe image of the neonlike $J=0-1$ Ti and Cr x-ray lasers. Prepulse level 15%. Double slit horizontally oriented with 80-μm slit spacing. The image demonstrates the deterioration of the fringe contrast at angles away from the peak emission angle.

[1]Fabricated by Fenzl Spezialleuchten, D-33813 Oerlinghausen.

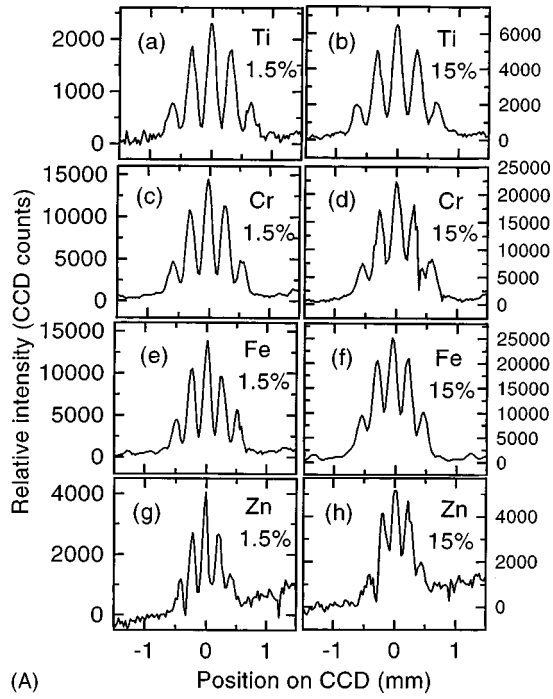

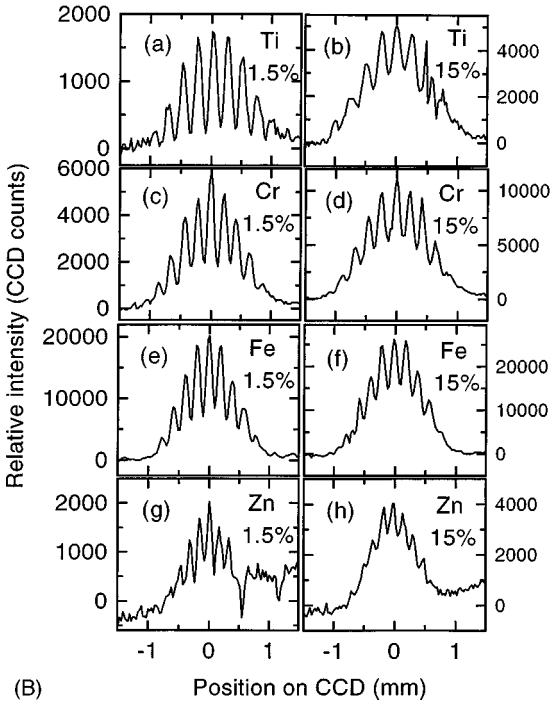

FIG. 4. Spectra of the fringe pattern at the peak of the emission for Ti, Cr, Fe, and Zn for 1.5% and 15% prepulse levels. The double slits are horizontally oriented. (A) Slit separation 80 μm. (B) Slit separation 110 μm.

and 23.6-nm lines are not resolved. However, since the relative wavelength separation is only 1.7%, an appreciable loss in fringe contrast is not expected.

To evaluate the data, we note that the coherence of a light source is characterized by its mutual intensity, which can be normalized to yield the complex coherence factor [29]. For ideal double-slit interference, in which both slits are uniformly illuminated (closely approximated by our experiment), the modulus of the complex coherence factor is equal

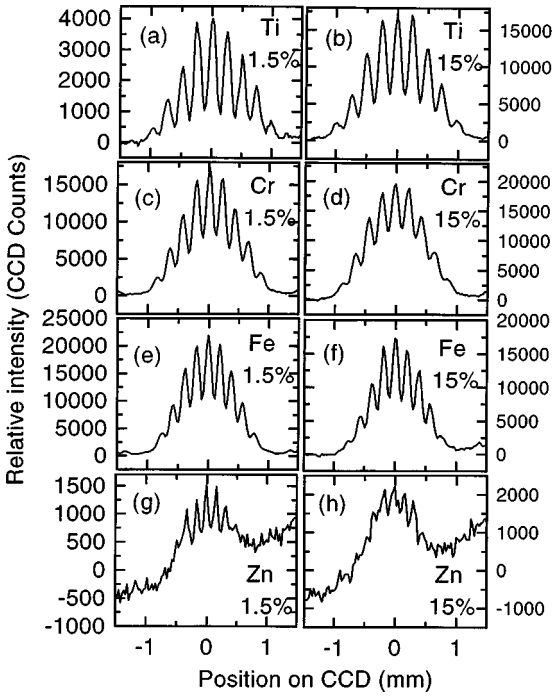

FIG. 5. Same as Fig. 4, but with slits vertically oriented. The slit separation is 110 μm.

to the fringe visibility, defined as

$$|\mu| = (I_{\max} - I_{\min})/(I_{\max} + I_{\min}), \tag{1}$$

where $I_{\max}$ and $I_{\min}$ are the maximum and minimum intensities of the fringe pattern. Thus one can directly derive information about the spatial coherence of the x-ray laser by measuring the fringe visibility.

From the fringe visibility as a function of slit spacing, the equivalent incoherent source size of the x-ray lasers can be calculated. For the simple assumption of an incoherently radiating circular disk, the Van Cittert-Zernike theorem results in the modulus of the complex coherence factor as given by

$$|\mu(\Delta x)| = 2\frac{J_1(\pi d_s \Delta x/\lambda z)}{\pi d_s \Delta x/\lambda z}, \tag{2}$$

where Δx is the slit spacing, d_S is the diameter of the source, z is the distance from the source to the double slit, and J_1 is the Bessel function of the first kind, order 1.

The evaluation of our data, using the above expression, is shown in Figs. 7(a)–7(d) for Ti, Cr, Fe, and Zn, and in Fig. 8 for Ge. In all of these diagrams the solid circles and squares represent data for the vertical spatial coherence of x-ray lasers obtained with 1.5% and 15% prepulse levels, and the open circles and squares correspond to the horizontal spatial coherence with the same prepulse levels. The dashed and dotted curves give the fringe visibility, calculated from the emission of an incoherent disk, the diameter of which is matched to the data. For the data with two slit separations this model gives reasonable agreement with the observed visibility as a function of slit spacing.

The incoherent source diameters derived this way are listed in Table I. The values for the horizontal direction (perpendicularly to the target surface), and the values for germa-

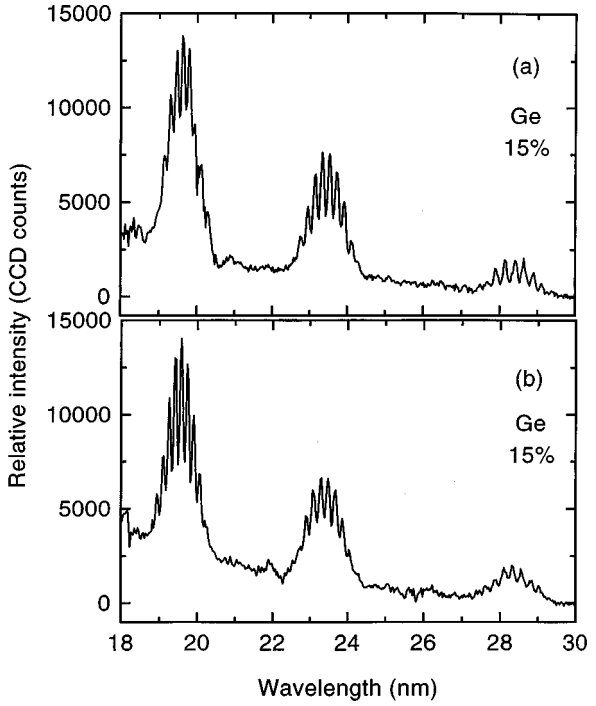

FIG. 6. Interference fringe patterns for Ge. The figures show the $J=0-1$ line at 19.6 nm, the $J=2-1$ lines at 23.2 and 23.6 nm (not resolved), and a $J=2-1$ line at 28.6 nm. (a) Slits horizontally oriented. (b) Slits vertically oriented. The prepulse level is 15% in both cases. The horizontal axis displays the wavelength instead of the position on the CCD (as in Figs. 4 and 5) to indicate the different emission lines of the germanium x-ray laser.

nium are written in parentheses since they are derived from a single-slit spacing only. All effective incoherent source sizes are less than the width of the line focus, except for the vertical size of the Ti laser obtained for a prepulse level of 15%. Quite generally, in the vertical direction the equivalent incoherent source sizes are smaller for the lower prepulse level. In the horizontal direction there is much less difference between the two prepulse levels. It is also interesting to note that the effective source sizes are quite similar for all four lasers in the case of a 1.5% prepulse, whereas they increase toward lower Z with the 15% prepulse (see Sec. IV below). The results indicate that a high prepulse level increases the intensity of an x-ray laser (compare the different counts in Fig. 4), but adversely affects the spatial coherence.

Turning now to germanium we note that for the (23.2, 23.6)-nm line doublet the horizontal and vertical coherences are quite comparable, whereas the 19.6-nm line is more coherent in the horizontal direction. The horizontal coherence for the 19.6-nm line is significantly higher than the one of the (23.2, 23.6)-nm lines, which confirms recently published results [18].

The equivalent incoherent source sizes can be compared to the measured near-field emission patterns of the x-ray lasers. To record near-field patterns, the x-ray laser emission was imaged in the vertical direction by focusing with a cylindrical mirror onto the CCD camera. For horizontal imaging a 50-μm vertical slit was used. Available data for 15% and 1.5% prepulse levels include Ti, Fe, Cu, and Ge, as shown in Fig. 9. Note the different horizontal and vertical scales resulting from the different magnifications in these

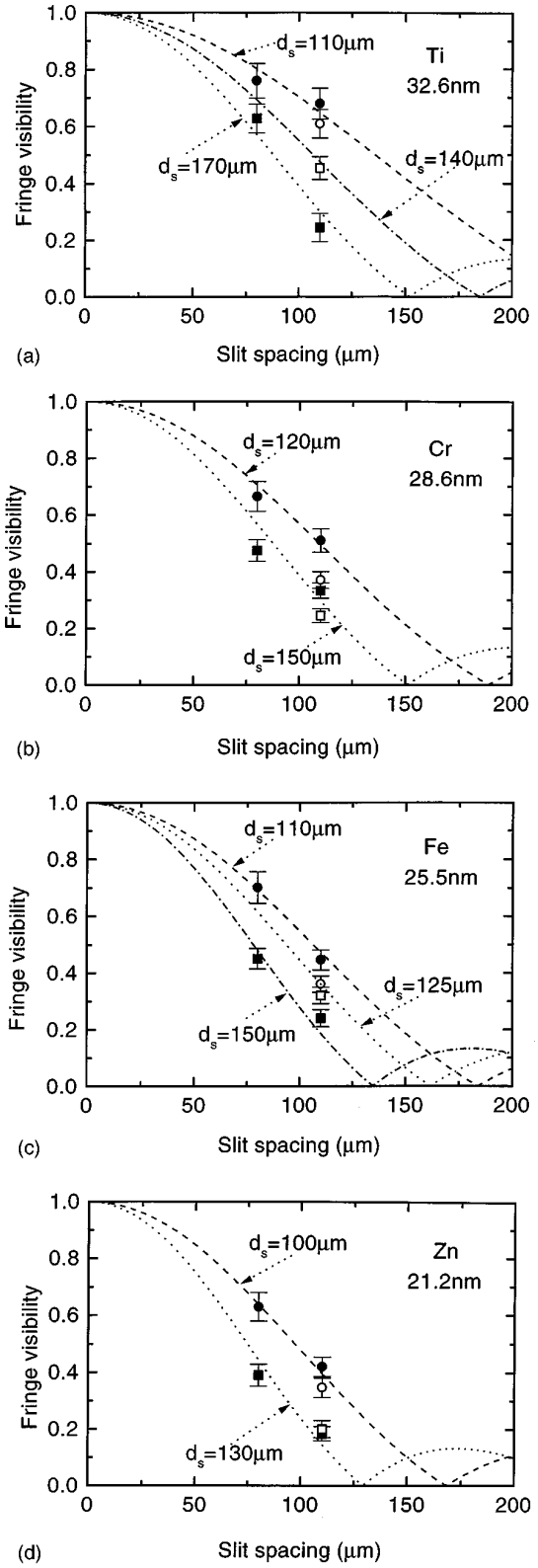

FIG. 7. The fringe visibility of neonlike (a) Ti, (b) Cr, (c) Fe, and (d) Zn $J=0-1$ x-ray lasers with different prepulse levels (1.5% and 15%) as a function of slit spacing. The *solid* circles and squares represent data for the vertical spatial coherence of x-ray lasers obtained with 1.5% and 15% prepulse levels. The *open* circles and squares represent data for the horizontal spatial coherence of x-ray lasers obtained with 1.5% and 15% prepulse levels. The dashed, dash-dotted, and dotted lines are curves according to Eq. (2), with the source diameter d_S matched to fit the data.

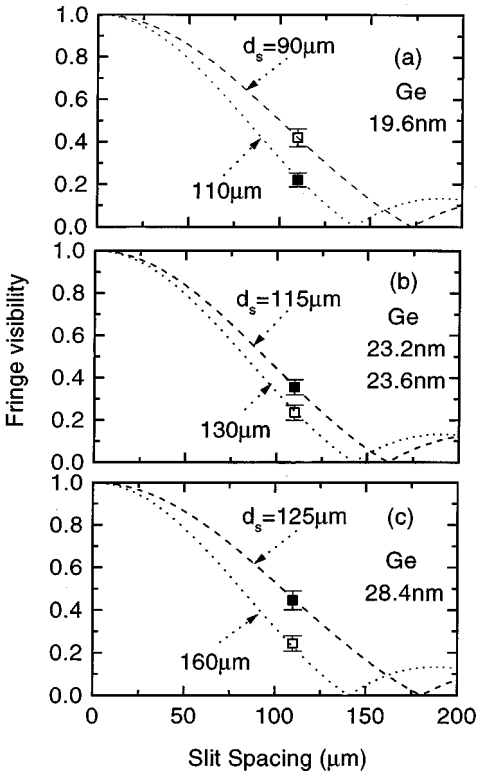

FIG. 8. Fringe visibility of neonlike Ge laser lines. Solid squares: data points for vertical spatial coherence. Open squares: data points for horizontal spatial coherence.

directions. All near-field patterns show considerable structure, in accord with previous findings at our and other laboratories [30,31]. In some cases a vertical splitting of the pattern into two spots 150–200 μm apart is observed. The structure is attributed to inhomogeneities in the intensity distribution transversely to the direction of the line focus [30].

Quite generally, it can be noted that the effective incoherent source sizes from Table I are somewhat smaller than the extension of the near-field patterns for the vertical as well as horizontal directions. We mention again that the coherence data in the horizontal direction are less reliable than the data for the vertical direction, since only a single-slit spacing was used.

TABLE I. Equivalent incoherent source diameters d_S for vertical and horizontal coherences and 1.5% and 15% prepulse levels. Values in parentheses are obtained with a single slit spacing.

	d_S (μm)			
	Vertical		Horizontal	
	1.5%	15%	1.5%	15%
Ti (32.6 nm)	110	170	(110)	(140)
Cr (28.5 nm)	120	150	(140)	(160)
Fe (25.5 nm)	125	150	(125)	(130)
Zn (21.2 nm)	100	130	(110)	(125)
Ge (19.6 nm)		(110)		(90)
Ge (23.2/23.6 nm)		(115)		(130)
Ge (28.6 nm)		(125)		(160)

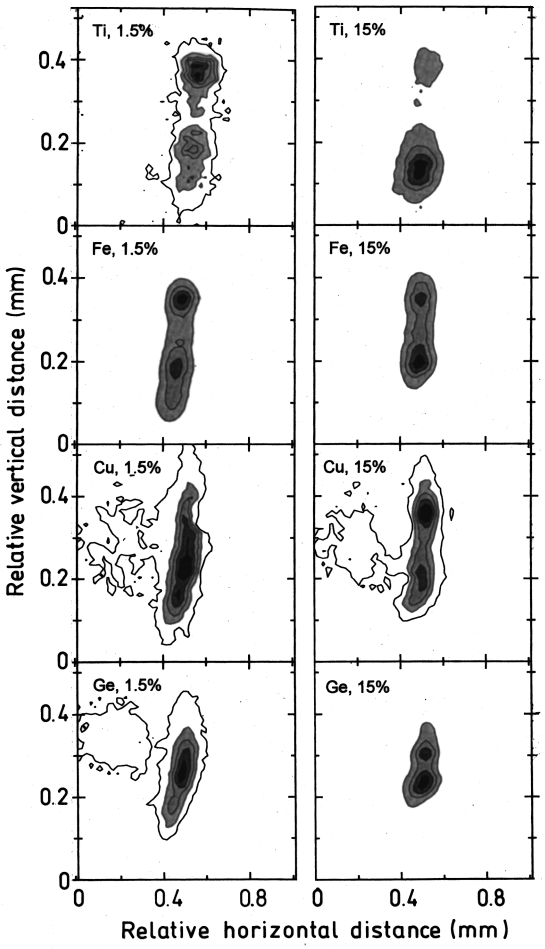

FIG. 9. Experimental near-field patterns for Ti, Fe, Cu, and Ge. Horizontal and vertical directions refer to the coordinate system shown in Fig. 1.

IV. SIMULATIONS AND DISCUSSION

To understand the above findings, in particular the observation that a lower prepulse level results in a higher degree of coherence, we performed simulations of a prepulse-induced x-ray laser for the two prepulse levels. Simulations of prepulse induced lasing for various prepulse levels have been previously carried out for germanium [32].

It is clear that a full account of the effects of plasma expansion in a direction parallel to the target surface is only possible by means of a 2D simulation. Usually, the two dimensionality of the problem is approximated by assuming cylindrical geometry with a prescribed expansion angle or by treating the transverse expansion of the plasma with a self-similar analytic solution (1.5D model). The importance of multidimensional modeling has been discussed in the literature [33].

True 2D simulations of the x-ray laser plasma were performed by MULTI2D, a code recently developed at our institute to simulate laser-irradiated cavities [34,35]. It solves fluid motion by means of a fixed Eulerian grid formed by triangular elements and includes two-dimensional radiation transport. The simulations were carried out for copper due to the availability of the opacity tables required for the treatment of radiation transport.

The two-dimensional electron density and temperature

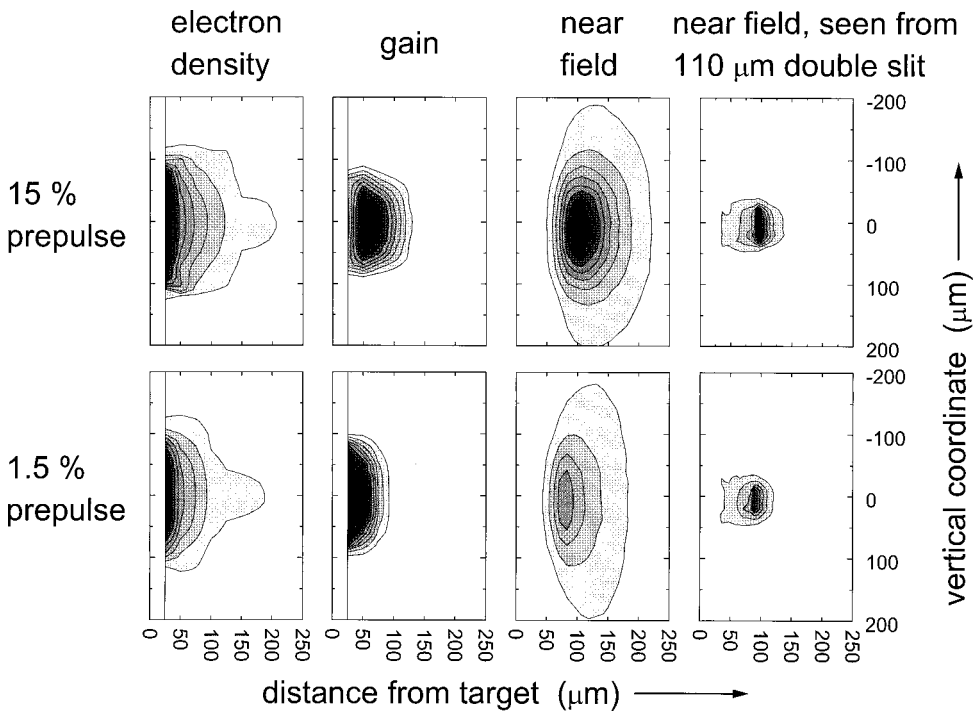

FIG. 10. Simulation results for copper. Contour plots of electron density, gain coefficient, and full-angle and narrow-angle near-field patterns for 1.5% and 15% prepulses. The fractional change from contour to contour is 10% of the peak value. The highest value of electron density is 4.5×10^{20} cm^{-3}. The normalization is the same for the 1.5% and 15% prepulse cases.

distributions were calculated for a focus width of 150 μm with a linear ramp of 10 μm at the edges. In accord with the experiments, a main pulse intensity of 20 TW/cm^2 and 1.5% and 15% prepulses were used. Prepulses and main pulses were assumed to be of a sin^2 temporal shape (a full width at half maximum of 500 ps) with the pulse maxima 5 ns apart. The x-ray laser gain was calculated using a simple gain model based on Elton's scaling laws [36] modified to take the spatial temperature variation into account, viz.

$$g = g_0(1-0.5N_e/N_{e,\mathrm{opt}})\exp(-\Delta E/kT_e). \qquad (3)$$

The prefactor g_0 was adjusted to yield the experimental gain coefficient. In Eq. (1), $N_{e,\mathrm{opt}}$ is the optimum electron density, given by $N_{e,\mathrm{opt}}=4\times10^{15}\ (Z-9)^{3.75}$ cm^{-3} (3×10^{20} cm^{-3} for copper), ΔE is the excitation energy of the upper laser level, and kT_e is the electron temperature.

A ray tracing code was used as a postprocessor, with gain and refractive index distributions obtained from the hydrocode. The refractive index distribution was assumed to be determined entirely by the contribution of the free-electron gas, i.e., the refractive index was calculated as $n=1-N_e/2N_c$, where N_e and N_c are the electron density and the critical electron density, respectively. Initial conditions of the Monte Carlo type were assumed, i.e., a statistical distribution of ray origins, weighted with ion density, and statistical initial directions.

Results of the simulations at the time of the x-ray laser pulse maximum (4.9 ns after the prepulse maximum) are shown in Fig. 10. The figure displays contour plots of the electron density and the gain coefficient, as well as two kinds of near-field patterns. The first near-field distribution is the one which would be recorded by collecting the emission by means of an optical system with a large aperture, e.g., a toroidal mirror. The other one is the spatial distribution of rays which eventually hit the region between and including the double slit with 110-μm separation.

Comparing first the large-angle–near-field patterns for the two prepulses, we see that the main experimental observations are qualitatively well reproduced, specifically the greater distance of the emitting region from target and the higher output intensity with a higher prepulse level. In keeping with experiment, the shape of the near-field pattern is elongated along the direction parallel to the target surface, indicating that only a relatively narrow region is contributing to the emission. Another feature in agreement with experimental results is the fact that the emission occurs farther from the target than the gain region [37].

We note, however, that the predicted distance of the lasing region from target is lower than the experimental one [38]. Except for g_0, no adjustable parameters are used in the simulations, and a better quantitative agreement could be obtained by using a lower value for $N_{e,\mathrm{opt}}$. Another deviation from experimental observation is that the doubly peaked structure of the near-field patterns is not reproduced by the simulations. We attribute this to the simplification implicit in the assumption of a flat intensity distribution across the line focus.

Nevertheless, the simulations help to understand the different degrees of coherence for the 1.5% and 15% prepulses. Comparing the electron-density distributions for the two prepulse levels, the distribution for the 1.5% prepulse case appears to be smooth, whereas that for the 15% prepulse shows the onset of a lateral shock wave resulting in a high vertical electron-density gradient. This behavior is indicative of the onset of turbulence at the higher prepulse level, an interpretation confirmed by our futile attempts to perform the

corresponding 2D simulations for iron. For this material, the 1.5% prepulse level still yielded a smooth electron-density distribution, whereas a 15% prepulse invariably resulted in numerical instability of the code. Apparently, the impact of the main pulse on the larger preplasma led to turbulence which could not be handled by the numerics.

A comprehensive assessment of coherence is, of course, not possible by ray tracing. However, ray tracing can give information on certain aspects of coherence, especially on the improvement of transverse coherence by a gain medium [39]. Enhanced coherence is associated with a narrow emission area at a particular angle, a quantity amenable by ray tracing. If the directional pattern of the emission is peaked on axis, a higher degree of coherence is expected.

To apply this idea to our problem, the near-field patterns as seen from the double slit have been calculated and are displayed in the right part of Fig. 10. If they indicate the degree of coherence, there should be a difference in the size of the pattern for a 1.5% and 15% prepulse. In comparing the corresponding patterns, it is seen that indeed the near-field pattern for the 1.5% prepulse case is narrower than the one for a 15% prepulse. Thus the ray-tracing calculations are consistent with our experimental observations. They tell us that, in the low-prepulse case, coherence is enhanced by refraction: As the rays diverge, the apparent coherence on axis is increased [40]. On the other hand, a certain loss of coherence in the vertical direction at a high prepulse level may be due to lateral density variations, which cause a ''mixing'' of x-ray directions, resulting in a larger apparent area of the axial emission. Note, however, that the effect of ''hosetype'' density fluctuations, caused by a nonuniform intensity distribution along the line focus [41], cannot be treated by our simulations, since it would require a three-dimensional analysis.

V. CONCLUSION

Measurements of the transverse spatial coherence for prepulse-induced low-Z neonlike $J=0-1$ x-ray lasers for 1.5% and 15% prepulses show that higher spatial coherence is obtained with a lower prepulse level. Furthermore, comparing the emission with that of an incoherent radiating disk, the effective incoherent source size turns out to be smaller than that of the experimental near-field pattern. Numerical simulations of a prepulse-induced Cu laser for the two prepulse levels reproduce many experimental features such as a higher emission intensity and a greater distance of lasing from the target with a higher prepulse level. The erratic structure of the experimental near-field patterns is not seen in the simulations, and is attributed to variations in the pump intensity across the line focus. The experimentally observed higher coherence for a 1.5% prepulse is also predicted by the simulations. The effect is interpreted as being due to refraction of rays out of the plasma, thus resulting in an apparently smaller source size.

ACKNOWLEDGMENTS

The authors would like to thank the Asterix facility crew for providing support for the experiments. Special thanks go to W. Fölsner for preparing the double slits. P. L. was supported by the Alexander-von-Humboldt Foundation; he thanks Dr. K.-L. Kompa and his colleagues at MPQ for their hospitality. Y. L. was supported within the framework of the agreement between the Max-Planck-Society and Academia Sinica. G. P. was supported by the European Union-Programme ''HCM.'' This work was supported in part by the Commission of the European Communities in the framework of the Association Euratom–Max-Planck-Institut für Plasmaphysik.

[1] D. L. Matthews, P. L. Hagelstein, M. D. Rosen, M. J. Eckart, N. M. Ceglio, A. U. Hazi, H. Medecki, B. J. MacGowan, J. E. Trebes, B. L. Whitten, E. M. Campell, C. W. Hatcher, A. M. Hawryluk, R. L. Kauffman, L. D. Pleasance, G. Rambach, J. H. Scofield, G. Stone, and T. A. Weaver, Phys. Rev. Lett. **54**, 110 (1985).

[2] M. D. Rosen, P. L. Hagelstein, D. L. Matthews, E. M. Campell, A. U. Hazi, B. L. Whitten, B. J. MacGowan, R. E. Turner, and R. W. Lee, Phys. Rev. Lett. **54**, 106 (1985).

[3] R. C. Elton, *X-Ray Lasers* (Academic, San Diego, 1990).

[4] See, for example, papers in *X-Ray Lasers 1996*, edited by S. Svanberg and C-G. Wahlstrom, IOP Conf. Proc. No. 151 (Institute of Physics and Physical Society, Bristol, 1996).

[5] J. Nilsen, B. J. MacGowan, L. B. Da Silva, and J. C. Moreno, Phys. Rev. A **48**, 4682 (1993).

[6] J. Nilsen, J. C. Moreno, B. J. MacGowan, and J. A. Koch, Appl. Phys. B: Photophys. Laser Chem. **57**, 309 (1993).

[7] Y. Li, P. Lu, G. Pretzler, and E. E. Fill, Opt. Commun. **133**, 196 (1997).

[8] Y. Li, G. Pretzler, and E. E. Fill, Phys. Rev. A **52**, R3433 (1995).

[9] B. Rus, A. Carillon, B. Gauthe, P. Goedtkindt, P. Jaeglé, G. Jamelot, A. Klisnick, A. Sureau, and P. Zeitoun, J. Opt. Soc. Am. B **11**, 564 (1994).

[10] J. Nilsen and J. C. Moreno, Phys. Rev. Lett. **74**, 3376 (1995).

[11] P. Jaeglé, S. Sebban, A. Carillon, G. Jamelot, A. Klisnick, P. Zeitoun, B. Rus, F. Albert, and D. Ros, in *X-Ray Lasers 1996* (Ref. [4]), pp. 1–8.

[12] J. Zhang, P. J. Warwick, E. Wolfrum, M. H. Key, C. Danson, A. Demir, S. Healy, D. Kalantar, N. S. Kim, C. L. S. Lewis, J. Lin, A. MacPhee, D. Neely, J. Nilsen, G. J. Pert, R. Smith, G. J. Tallents, and J. S. Wark, Phys. Rev. A **54**, R4653 (1996).

[13] L. B. Da Silva, T. W. Barbee, Jr., R. Cauble, P. Celliers, D. Ciarlo, S. Libby, R. A. London, D. Matthews, S. Mrowka, J. C. Moreno, D. Ress, J. E. Trebes, A. S. Wan, and F. Weber, Phys. Rev. Lett. **74**, 3991 (1995).

[14] J. E. Trebes, S. B. Brown, E. M. Campbell, D. L. Matthews, D. G. Nilson, G. F. Stone, and D. A. Whelan, Science **288**, 517 (1987).

[15] K. A. Tanaka, Y. Kato, S. Nakai, K. Shinohara, T. Hond, L. Kodama, H. Iwasaki, T. Yoshinobu, T. Tsukamoto, M. Niibe, Y. Fukuda, D. Neely, A. MacPhee, and G. Slark, J. X-Ray Sci. Technol. **5**, 105 (1995).

[16] F. Albert, B. Rus, Ph. Zeitoun, A. Carillon, P. Jaeglé, G.

Jamelot, A. Klisnick, D. Ros, and S. Sebhan, in *X-Ray Lasers 1996* (Ref. [4]), pp. 427–429.

[17] J. Krishnan, C. Cairns, L. Dwivedi, M. Holden, M. H. Key, C. L. S. Lewis, A. MacPhee, D. Neely, P. A. Norreys, G. J. Pert, S. A. Ramsden, C. G. Smith, G. J. Tallents, and J. Zhang, in *X-Ray Lasers 1994*, Fourth International Colloquium held in Williamsburg, VA, May 1994, edited by D. C. Eder and D. L. Matthews, AIP Conf. Proc. No. 332 (AIP, New York, 1994), pp. 483–487.

[18] R. E. Burge, G. E. Slark, M. T. Browne, X.-C. Yuan, P. Charalambous, X.-H. Cheng, C. L. S. Lewis, A. MacPhee, and D. Neely, J. Opt. Soc. Am. B **14**, 2742 (1997).

[19] J. E. Trebes, K. A. Nugent, S. Mrowka, R. A. London, T. W. Barbee, M. R. Carter, J. A. Koch, B. J. MacGowan, D. L. Matthews, L. D. Da Silva, G. F. Stone, and M. D. Feit, Phys. Rev. Lett. **68**, 588 (1992).

[20] J. Trebes, in *X-Ray Lasers 1992*, edited by E. Fill, IOP Conf. Proc. No. 125 (Institute of Physics and Physical Society, Pittsburgh, 1993), pp. 265–268.

[21] M. C. Marconi, J. L. A. Chilla, C. H. Moreno, B. R. Benware, and J. J. Rocca, Phys. Rev. Lett. **79**, 2799 (1997).

[22] M. H. Sher, S. J. Benerofe, J. F. Young, and S. E. Harris, J. Opt. Soc. Am. B **8**, 114 (1991).

[23] I. C. E. Turcu, I. N. Ross, M. S. Schulz, H. Daido, G. J. Tallents, J. Krishnan, L. Dwivedi, and A. Hening, J. Appl. Phys. **73**, 8081 (1993).

[24] T. Ditmire, E. T. Gumbrell, R. A. Smith, J. W. G. Tisch, D. D. Meyerhofer, and M. H. R. Hutchinson, Phys. Rev. Lett. **77**, 4756 (1996).

[25] J. Zhang, M. Zepf, P. A. Norreys, A. E. Dangor, M. Bakarezos, C. N. Danson, A. Dyson, A. P. Fews, P. Gibbon, M. H. Key, P. Lee, P. Loukakos, S. Moustaizis, D. Neely, F. N. Walsh, and J. S. Wark, Phys. Rev. A **54**, 1597 (1996).

[26] H. Baumhacker, G. Brederlow, E. Fill, Ch. Schrödter, R. Volk, S. Witkowski, and K. J. Witte, Laser Part. Beams **11**, 353 (1993).

[27] W. Chen, S. Wang, C. Mao, B. Chen, and A. Xu, in *1990 Conference on Laser and Electro-Optics*, Technical Digest Series Vol. 7 (Optical Society of America, Washington, DC, 1990), p. 282.

[28] K. A. Nugent and J. E. Trebes, Rev. Sci. Instrum. **63**, 2146 (1992).

[29] J. W. Goodman, *Statistical Optics* (Wiley, New York, 1985).

[30] J. C. Moreno, J. Nilsen, Y. Li, P. Lu, and E. E. Fill, Opt. Lett. **21**, 866 (1996).

[31] M. H. Key *et al.*, in *X-Ray Lasers 1996* (Ref. [4]), pp. 9–16.

[32] S. B. Healy, G. F. Cairns, C. L. S. Lewis, G. J. Pert, and J. A. Plowes, IEEE J. Sel. Top. Quantum Electron. **1**, 949 (1995).

[33] S. Jacquemot, L. Bonnet, and M. Nantel, in *X-Ray Lasers 1996* (Ref. [4]), pp. 269–273.

[34] R. Ramis and J. Meyer-ter-Vehn, Max-Planck-Institut für Quantenoptik Report No. MPQ-174 (unpublished).

[35] R. Ramis and J. Meyer-ter-Vehn, in *Proceedings of ECLIM 1994*, edited by S. J. Rose, IOP Conf. Proc. No. 140 (Institute of Physics and Physical Society, Bristol, 1995), pp. 97–100.

[36] R. C. Elton, *X-Ray Lasers*, p. 107.

[37] J. Nilsen, J. C. Moreno, T. W. Barbee, Jr., and L. B. Da Silva, *Soft X-ray Lasers and Applications*, edited by J. J. Rocca and L. B. Da Silva, SPIE Conf. Proc. No. 3156 (SPIE, San Diego, 1997), pp. 65–70.

[38] Y. Li, G. Pretzler, and E. E. Fill, Phys. Rev. A **51**, R4341 (1995).

[39] R. A. London, Phys. Fluids **31**, 184 (1988).

[40] O. Zahavi, G. Hazak, and Z. Zinamon, J. Opt. Soc. Am. B **10**, 271 (1993).

[41] P. Amendt, M. Strauss, and R. A. London, Phys. Rev. A **53**, R23 (1996).